Journal of
Marine Science and Engineering

MDPI

Article

Effect of Internal Waves on the Hydrodynamics of a Mediterranean Sea Strait

Nikolaos Th. Fourniotis

Department of Civil Engineering, University of the Peloponnese, 26334 Patras, Greece; nfou@uop.gr

Abstract: In the present work, the effects of wind- and tide-induced internal waves in the Rio-Antirio Strait in western Greece were studied by using three-dimensional numerical simulations. For the wind-induced flow in the strait, it emerged that the internal waves' initiation is associated with the direction of the wind. Tidal action, with or without the combined action of wind, also generates internal waves in the strait, with amplitudes higher than 20 m. The action of the internal waves causes a subsurface inflow of colder waters from the Gulf of Corinth to the Gulf of Patras, as has been also simulated for the case of the wind-induced flow, generating strong hypolimnetic currents. The exchange flowrate between the Gulf of Patras and the Gulf of Corinth appeared to undergo significant modification for the wind-induced flow and had little effect for the pure tidal flow (in windless conditions) due to the development and action of the internal waves at the strait. The combined action of the tide and the wind was found to marginally affect the exchange flowrate between the two gulfs compared to the pure tidal flow. The interaction between the Coriolis effect and internal waves, at least away from the strait, forms a characteristic horizontal structure of flow. The structure of turbulence in the near strait area under the action of internal waves generated by the wind and/or tide was also discussed and compared with the corresponding barotropic flow.

Keywords: coastal circulation; internal waves; strait; stratification; tidal circulation; wind-induced circulation

check for updates

Citation: Fourniotis, N.T. Effect of Internal Waves on the Hydrodynamics of a Mediterranean Sea Strait. *J. Mar. Sci. Eng.* **2024**, *12*, 532. https://doi.org/10.3390/jmse12040532

Academic Editor: Anatoly Gusev

Received: 1 February 2024
Revised: 17 March 2024
Accepted: 19 March 2024
Published: 23 March 2024

Copyright: © 2024 by the author. Licensee MDPI, Basel, Switzerland. This article is an open access article distributed under the terms and conditions of the Creative Commons Attribution (CC BY) license (https://creativecommons.org/licenses/by/4.0/).

1. Introduction

Internal waves are gravity waves in the interior of the sea flow, and they propagate in fluids with stable density stratification [1]. These waves are observed at the interface between the upper low-density water layer and a bottom higher-density one [2] or, very often, they are observed to travel along a seasonal thermocline, far from the bottom layer. When a water body is thermally stratified, these wave-like oscillations are more easily detected by the rise and fall of isotherms [3]. The first scientific observations of internal waves were reported by the Norwegian explorer Fridtjof Nansen in the last decade of the nineteenth century [4], as cited by Leder [5]. These waves are of high importance as they play a significant role in marine hydrodynamic processes, such as the transport of nutrients and sediment as well as mixing processes and turbulence intensity in the water column. Internal waves are characterized by further complication. Many types of these can contribute to the local mixing at the generation site or to the mixing enhancement at remote locations, as they can also transport their energy over long distances [6]. In addition, they can evolve into internal hydraulic jumps [2,7].

Regarding basic hydrodynamic parameters, internal waves can have horizontal currents with magnitudes of up to 1 m/s and, thus, are strong enough to significantly affect the navigation of vessels [8]. Vertical currents of internal waves can reach 0.5 m/s, posing significant problems in subsurface navigation and structures, such as those associated with offshore energy development [9]. The most common driving force of the generation of internal waves is tide. Another mechanism that can also contribute to the generation of internal waves is the interaction of marine flows with underwater sills, leading to the

generation of lee waves. Specifically, in the presence of stratification, the formation of internal waves is expected in a silled strait [10,11]. Moreover, internal waves can also be generated under the effect of wind. Wind-generated internal waves have been widely studied and it has been demonstrated that the divergence and convergence of wind velocity, as well as time–space-varying wind field, can excite baroclinic instabilities [12–14]), as cited by Koohestani et al. [15].

The generation of internal waves in strait sites is nearly a common phenomenon caused by both wind and tidal action, as well as their interaction with strait geometry and topographical effects. Wang et al. [16] have studied the internal waves in the Strait of Georgia based on a large number of satellite remote sensing images and the application of statistical analysis. Khimchenko et al. [17] have analyzed measurements of isotherm fluctuations and applied the global tidal model in the Bransfield Strait (Antarctica) in order to study the characteristics of internal waves. Purwandana et al. [18] have studied the internal solitary waves in the Lombok Strait (Indonesia) by examining the formation as well as the characteristics of waves away from the generation site. Brandt et al. [19] have carried out high-resolution oceanographic measurements in the Strait of Messina. These measurements were found to represent a detailed picture of the tidally induced internal dynamics in the Strait of Messina during the period of investigation, contributing to elucidating several aspects of the general internal dynamics in the area. Vlasenko et al. [20] have investigated the horizontal and vertical structure of large-amplitude internal solitary waves propagating in stratified waters on a continental shelf, analyzing the results of numerical simulations and in situ measurements of high-resolution in situ data acquired north and south of the Strait of Messina in the Mediterranean Sea.

Furthermore, the effect of internal waves on biological parameters has also been examined by many researchers in both marine and freshwater environments. Sangra et al. [21] have carried out a physical and biological survey in the shelf break region located southwest of Gran Canaria Island to investigate the effect of internal waves on the abundance and distribution of phytoplankton. In addition, Rinke et al. [22] have investigated the effect of wind-induced internal waves on the vertical distribution of zooplankton in Bautzen Reservoir (Saxony, Germany), while Garwood et al. [23] have reviewed the biological impacts of non-breaking internal waves for three broad categories of organisms: sessile organisms, passive plankton, and depth-keeping plankton.

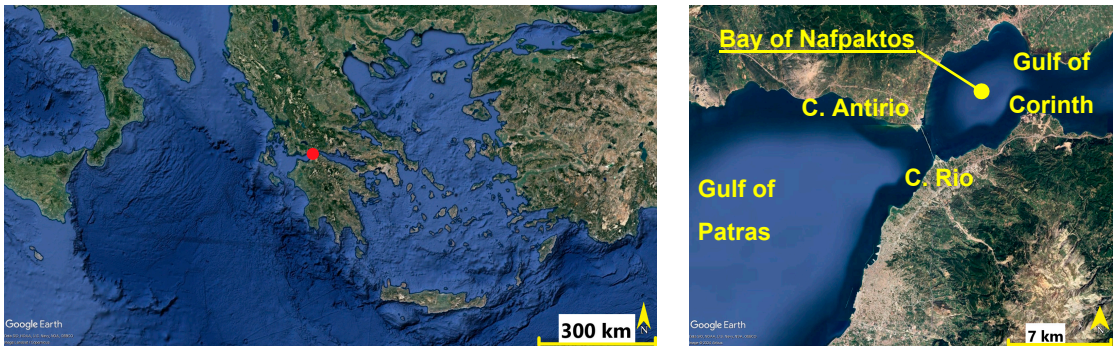
In the semi-enclosed microtidal Mediterranean Sea, the presence of straits and channels is a crucial parameter for the hydrodynamic circulation of the Mediterranean basin. In particular, internal waves and internal tides recorded in the Mediterranean straits substantially affect the hydrodynamics of the seas: in the Strait of Gibraltar at the Camarinal Sill [24–29]); in the Messina Strait [30–35]; and in the eastern Sicily channel [36]. In the Greek seas, Drakopoulos and Lascaratos [37] studied the internal tides near the Strait of Rio in Greece; they explored their generation and propagation characteristics, taking into account the influence of upwelling events. Rubi et al. [38] have investigated the combined effects of tidal currents and internal tides on the current pattern of the Strait of Rio (Greece) as well as on the sea bottom of the strait, and they also examined the hydro-sedimentary processes in the strait area. Their study was based on satellite images and on an oceanographic survey; they concluded that the Rio Strait is dominated by erosional, rather than depositional, features and that the occurrence of an internal tide from the Corinth Gulf generates strong bottom currents and upwelling events.

In the current study, the effect of wind- and tide-induced internal waves on the hydrodynamics of the wider area associated with the Mediterranean Sea strait of Rio-Antirio is examined with emphasis on the exchange flowrate that takes place in this strait. To this purpose, numerical simulations were performed utilizing a CFD code. The understanding of this complex flow is expected to be crucial for the local hydrodynamics of the adjustment gulfs. The magnitude of the exchange flowrate as well as the consequent flow structure of the area are expected to significantly affect the local environmental processes, as well as the water renewal in the shallower Gulf of Patras, which is connected to the larger and deeper

Gulf of Corinth through the strait of Rio-Antirio. Additionally, the effect of internal waves on the structure of the flow and turbulence development is discussed, while numerical predictions are compared with the corresponding barotropic flow.

1.1. Area of Interest and Available Studies

The Rio-Antirio strait is located between central Greece and the Peloponnese (Figure 1). It is a relatively shallow, flow-through Mediterranean silled strait (max depth ~70 m) and connects the deeper Gulf of Corinth in the east to the shallower Gulf of Patras in the west. The water masses of the strait area are exchanged under the effect of tide and wind from the Gulf of Patras to the Gulf of Corinth and vice versa, while between capes Rio and Antirio, a 2.6 km long cable-stayed bridge links western Greece with the Peloponnese. On the east of the wider area of the strait lies the Bay of Nafpaktos, which is adjacent to the western end of the Gulf of Corinth.



(**a**) (**b**)

Figure 1. (**a**) Part of the Eastern Mediterranean Sea. The wider area of the Rio-Antirio strait is marked with a red circle. (**b**) Wider area of Rio-Antirio strait including parts of the adjacent seas, the Gulf of Patras (in the west), and the Gulf of Corinth (in the east). Note: Bay of Nafpaktos is located in the western tip of the Gulf of Corinth. (Google Earth, 2024) [39].

Apart from field measurements and/or the analysis of satellite infrared images of the wider area of two gulfs [37,40–43], there are also detailed, local measurements that had been taken at the Rio-Antirio strait by Hadjitheodorou and Antonopoulos [44], Antonopoulos et al. [45,46], and Hadjitheodorou et al. [47] before the construction of the Rio-Antirio bridge. As documented by Hadjitheodorou et al. [47], the currents in the Rio-Antirio strait are among the strongest in Greece and are in the order of 1–1.5 m/s. The oscillatory nature of these currents makes it clear that they are dominated by the tidal flow, which is most strongly felt in the strait. Many of these measurements as well as the general structure of the flow hydrodynamics have been corroborated by a numerical study that regards the wider area of the Gulf of Patras, along with the adjacent Ionian sea on the west and the Bay of Nafpaktos on the east [48–51].

1.2. Wind Field Characteristics in the Wider Area of the Strait

The wind field that develops in the strait region varies drastically, since it is mainly influenced by the strong topography of the wider area [45]. In this work, numerical simulations are carried out for the case of wind shear stresses that are uniformly applied in terms of both space and time on the free surface.

The wind data given by Hatjitheodorou and Antonopoulos [44] have resulted from the processing of long-term observations of the weather stations situated at both Araxos (entrance of the Gulf of Patras) and University of Patras (nearby the area of Rio-Antirio strait), as well as from short-term observations of two additional stations installed at the location near the Rio-Antirio strait before the construction of the Rio-Antirio bridge. In the later study of Antonopoulos et al. [45], measurements of wind field provide the monthly

and annual mean wind frequencies observed in the strait area for a two-year period. There are also later wind records regarding the area of the Gulf of Patras that were received from the station of Araxos, and they indicate that wind directions and intensities are generally the same as the respective ones recorded in the past.

Generally, stronger winds blow from the east (northeast to east) and west sector, reaching up to 9 Bf (20.8–24.4 m/s) and 8 Bf (17.2–20.7 m/s), respectively. However, typical winds in the wider area of the Gulf of Patras do not exceed 3 Bf (3.4–5.4 m/s). The eastern sector, from northeast to southeast, includes the most frequent winds with approximately 52% of the total wind directions that blow in the area, followed by the western sector, from southwest to northwest, with approximately 30% of the total wind directions [44].

Based on the wind charts provided in the report of Papailiou [40], the strongest winds are southwesterly (SW), 225°, easterly (E), and northeasterly (NE) with directions from 90° to 45°. The prevailing winds are southerly (S), southwesterly (SW) to westerly southwesterly (WSW), as well as northerly (N), and northeasterly (NE) to easterly northeasterly (ENE), with average speed values of 3–5 m/s. Calm weather conditions occur with a frequency of about 35%, and this is the most frequent wind regime in the area, while the prevailing winds are NE, NW, W, and SW directions [52]. More specifically, the analysis of wind records that was based on direction and speed and was carried out in the period 1973–1992 shows that the average wind speed blowing in the wider area varies between 2 and 5 m/s, with the main direction covering the northeastern NE (45°) as well as the southwestern SW (225°) sector and acting nearly along the entire diagonal axis of the Gulf of Patras [45].

Based on the aforementioned information, the numerical simulations of the current study were carried out by applying a constant wind speed of 4 m/s that covered all prevailing directions. The main goal is to shed light on the structure of the pure wind-driven circulation in the wider area of the strait, as well as to study the combined action of wind and tide with emphasis on the understanding of the strait hydrodynamics in detail. It is highlighted that, under the influence of these light-wind conditions, no erosion of the thermocline is expected, even after several hours of wind action.

2. Methodology

2.1. Hydrodynamic Formulation

The numerical simulations were performed using the CFD code MIKE 3 Flow Model FM (hydrodynamic module) [53]. For the details of the code, the interested reader is referred to DHI [53]. This modeling system is based on a finite volume, unstructured mesh approach. The simulations were based on the solution of the Reynolds-averaged Navier–Stokes (RANS) equations for 3D unsteady and incompressible flow, invoking the Boussinesq assumption and the hypothesis of hydrostatic pressure in the vertical direction. In the horizontal plane, an unstructured mesh was used, while in the vertical direction, the discretization was structured. A sigma-coordinate transformation approach was used for the free surface management. For the turbulence closure, an eddy viscosity concept was used, described individually for the horizontal and vertical transport. More specifically, the Smagorinsky model [54] was used for horizontal subgrid-scale transport, while the standard k-ε turbulence model [55] was used for vertical eddy viscosity. To account for the Coriolis force, a variable Coriolis parameter f was used. An approximate Riemann solver scheme [56] was applied for spatial discretization.

2.2. Computational Domain, Boundary, and Initial Conditions

For the simulation of wind-induced barotropic (winter) circulation in the currently studied sea basin, which includes also the strait area, the computational domain, the open boundaries formation, as well as the initial and boundary conditions were identical to those applied in [49]. The study of the wind- and tide-induced baroclinic/barotropic circulation in the same sea basin was based on the studies of [50,51] in regard to the aforementioned parameters. In these author's works, the hydrodynamic circulation in

the wider area, including the strait, was thoroughly studied both for summer and winter regimes. More specifically, the resolution of the horizontal unstructured as well as the vertical structured mesh are shown in Figure 2. In the horizontal plane, a non-uniform computational mesh was generated, where the resolution was made finer close to the coasts and the grid size gradually increased up to 1000 m in the offshore region of the gulfs, leading to 10,169 elements in the horizontal (5378 nodes). In the vertical plane, 10 σ-layers over depth were used. A small time step of 4 s was required to satisfy the Courant–Friedrichs–Lewis (CFL) criterion and avoid divergence. The boundary vertical temperature and salinity profiles (density stratification) were set equal to the initial conditions and were kept constant in all simulations. More specifically, density stratification essentially resulted due to temperature stratification according to field data, since vertical salinity profiles were found to be nearly constant [40]. Thus, the initial condition of the stratification used for the simulations was constructed by averaging five typical vertical temperature profiles and calculating the corresponding density profile. In this calculation, the value of the salinity was set in accordance with the data, equal to 38.5 psu.

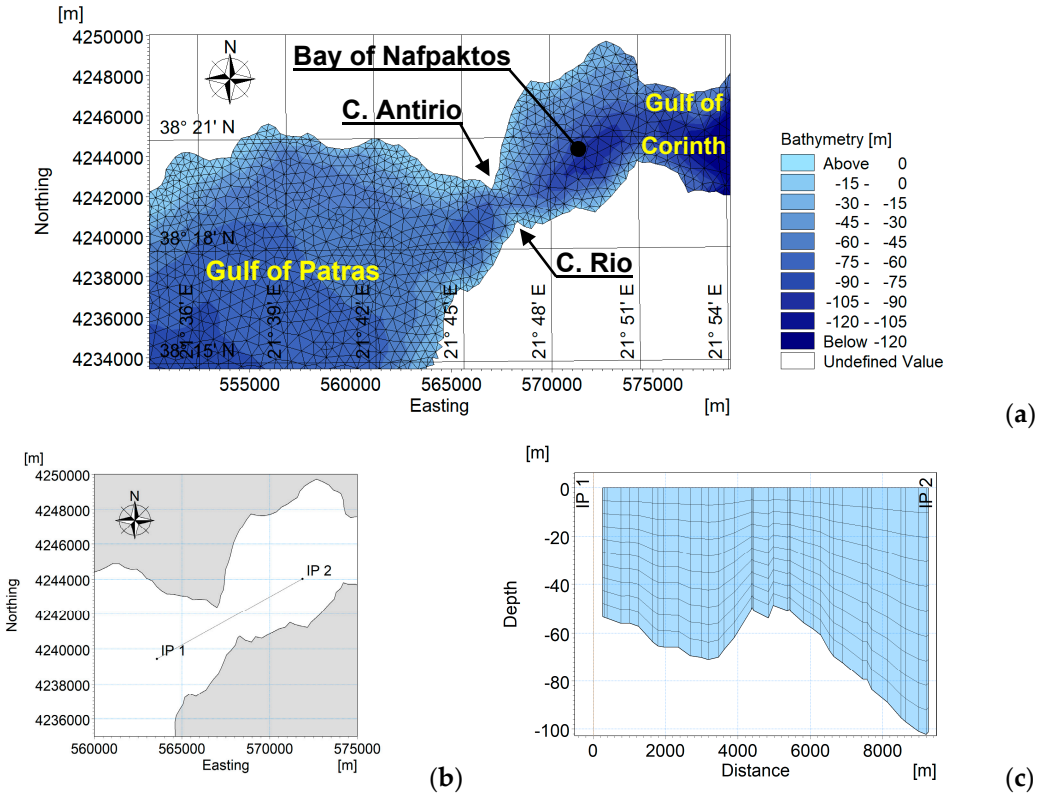


Figure 2. (**a**) Bathymetric map of the wider area of the strait, with isobaths shown every 15 m. The unstructured mesh is superimposed. (**b**) Line IP1-IP2 on the map of the strait, showing the location of vertical cross-section. (**c**) Longitudinal section along the strait corresponding to (**b**), where the vertical structured grid is shown.

The current study puts emphasis on the generation of internal waves in the strait as well as on their effect on flow hydrodynamics. All simulations were carried out using an Intel core i7, 3.4 GHz PC; it is noteworthy that the computation (running) time that was required for the hydrodynamic simulation of a 4-day period was equal to about 1.5 h.

3. Results and Discussion

3.1. Brief Presentation of Hydrodynamic Circulation in the Wider Area of the Rio-Antirio Strait

In this section, the basic hydrodynamic characteristics of the wider area of the strait are briefly summarized based on numerical model results. It is reminded that the area of

interest—also defined as the wider area of the strait of Rio-Antirio—includes part of the eastern Ionian Sea, the Gulf of Patras, the site of the strait, the Bay of Nafpaktos, and part of the western tip of the Gulf of Corinth. The hydrodynamic circulation in these areas has been studied using three-dimensional numerical simulations [48]. The Gulf of Patras is a relatively shallow, flow-through, Mediterranean basin opening into the Ionian Sea on the west, and through the strait of Rio-Antirio into the deeper Gulf of Corinth, on the east. During the summer period, thermal stratification exists in these waters, the presence of which affects the hydrodynamic circulation.

During the winter months, batotropic flow develops in the wider area of the strait. The simulations show that the wind-induced flow creates strong coastal currents in the Gulf of Patras. Strong wind-induced currents are also generated at the Rio-Antirio strait [49]. For the tide-induced circulation, the numerically predicted results indicate that strong tidal currents develop at the strait of Rio-Antirio and in the main body of the Gulf of Patras, with cyclonic and anticyclonic eddies being developed at the northern and southern coasts, respectively. In the case of wind blowing, nearshore gyres develop too; the sense of rotation of these gyres coincides with the wind direction, while in the central part of the gulf, the flow pattern is mainly dictated by the tidal action [51].

Furthermore, the baroclinic wind- and tide-induced circulations have been studied to examine the effect of stratification on the flow structure. Based on numerical simulations for the summer period, it was concluded that the wind-induced flow and the wind-generated turbulence driven by light winds are restricted to the surface well-mixed layer of the epilimnion [57]. However, the strong winds cause tilt and erosion of the thermocline in the main body of the Gulf of Patras [57], as well as the generation of internal waves at the Rio-Antirio strait. In addition, the numerical simulations predicted the characteristics of the baroclinic (summer) flow in the Gulf, which include strong upwellings and a central cyclonic gyre [50].

It is mentioned here that in the above simulations, as well as in the following results that put emphasis on the strait region, a hydrostatic model has been used. Internal waves are inherently non-hydrostatic, but they are frequently resolved quite well in 3D hydrostatic coastal circulation models. The effect of the hydrostatic model assumption on the simulation of internal waves has been thoroughly studied by many research works [58–62], where characteristic model–observation discrepancies—arising from the hydrostatic approximation—have been discussed in detail. However, despite this assumption, the model simulates the baroclinic circulation in the strait, allowing the representation of internal waves and simulating the temporal variations in water temperature [50]. It is worth noting that similar 3D phenomena have also been simulated in the work of Zamani and Koch [62], using the same code, namely MIKE 3 FM (HD). In the later work, it was concluded that the models simulate the observed temporal variations in water temperature reasonably well, despite the fact that hydrostatic models have been used. Based on the above discussion, regarding the effect of the hydrostatic approximation on the study of internal waves, the numerical simulations were applied to shed light on the effect of internal waves on the hydrodynamics of the Rio-Antirio strait, rather than for studying in detail the structure of these waves. In the later case, a non-hydrostatic model is required, which remains outside the scope of the current work; this is dedicated to an initial numerical approach for studying the bulk effect of wind and tide-induced internal waves in the strait.

3.2. Generation and Action of Internal Waves in the Rio-Antirio Strait

3.2.1. Wind-Induced Circulation

The wind-induced currents in the upper well-mixed layer of the epilimnion, i.e., the free-surface layer of the strait, are stronger during the stratification compared to currents that develop in barotropic flow regime for the same wind conditions (Figure 3a). This is because the wind energy is distributed within the epilimnion (at least for light-to-medium-strength winds). In this case, the metalimnion acts as a separator zone, dividing the water

body vertically in nearly three zones, whereas in the barotropic flow the wind energy is dispersed throughout the depth of the strait (Figure 3b).

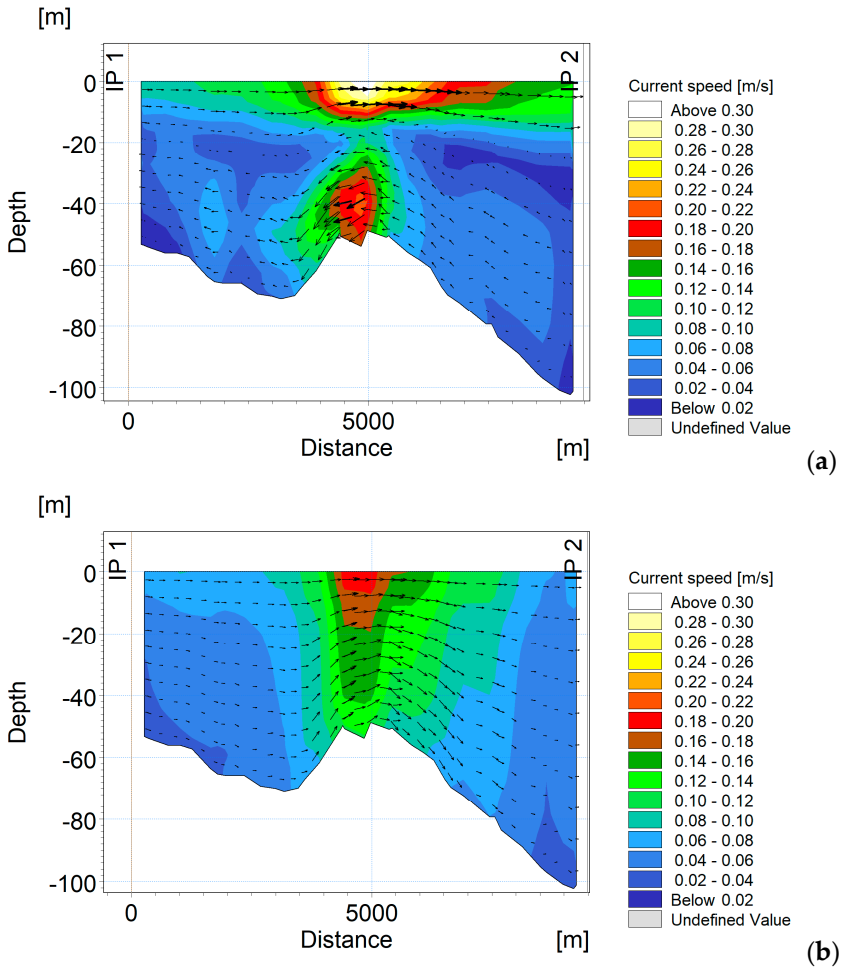


Figure 3. Vertical structure of the flow at the Rio-Antirio strait induced by a 4 m/s southwesterly (SW) wind, corresponding to IP1-IP2 section of Figure 2b, for (**a**) the summer and (**b**) the winter regime. Current speeds exceeding 0.2 m/s are marked with dark black arrows.

Under the stratification regime, an internal wave initiates in the area of the strait, approximately 6 h after the southwesterly (SW) wind stress is applied, as is revealed by the numerical simulations. This phenomenon causes a subsurface inflow of waters from the Gulf of Corinth to the Gulf of Patras, while in the surface layer, above the thermocline, the currents' direction is towards the Gulf of Corinth (as dictated by the wind action). More specifically, the action of the internal wave causes vertical circulation and leads to the reverse of the flow in the area below the thermocline in the hypolimnetic zone (Figure 3a). These subsurface currents were estimated to be quite strong, exceeding speed values of 0.2 m/s. The resultant flow structure leads to the inflow of colder bottom waters from the deeper Gulf of Corinth into the Gulf of Patras. At the free surface, under the wind action, warmer waters from the Gulf of Patras enter to the Gulf of Corinth through the Rio-Antirio strait. This reverse flow in the strait water column was estimated to significantly affect the exchange flowrate between the two gulfs.

In Figure 4, snapshots of the internal waves' motion at a cross-section along the strait are presented. It is shown that in the initial period, after the onset of the wind, the wind-induced flow affects the water column uniformly (Figure 4a), as in the case of barotropic wind-induced flow. A few hours later, the action of the internal wave leads to reverse subsurface (hypolimnetic) flow. While the amplitude of the internal wave

gradually increases, higher values of reverse subsurface currents are generated (Figure 4b). Subsequently, the amplitude of the internal wave decreases and almost stagnant waters appear in the hypolimnetic zone (Figure 4c). The motion of internal waves continues, leading to a reverse flow and the pumping of colder waters from the Gulf of Corinth to the Gulf of Patras. It is worth noting that the larger the amplitude of the internal wave, the stronger the generated subsurface reverse flow is (Figure 4d).

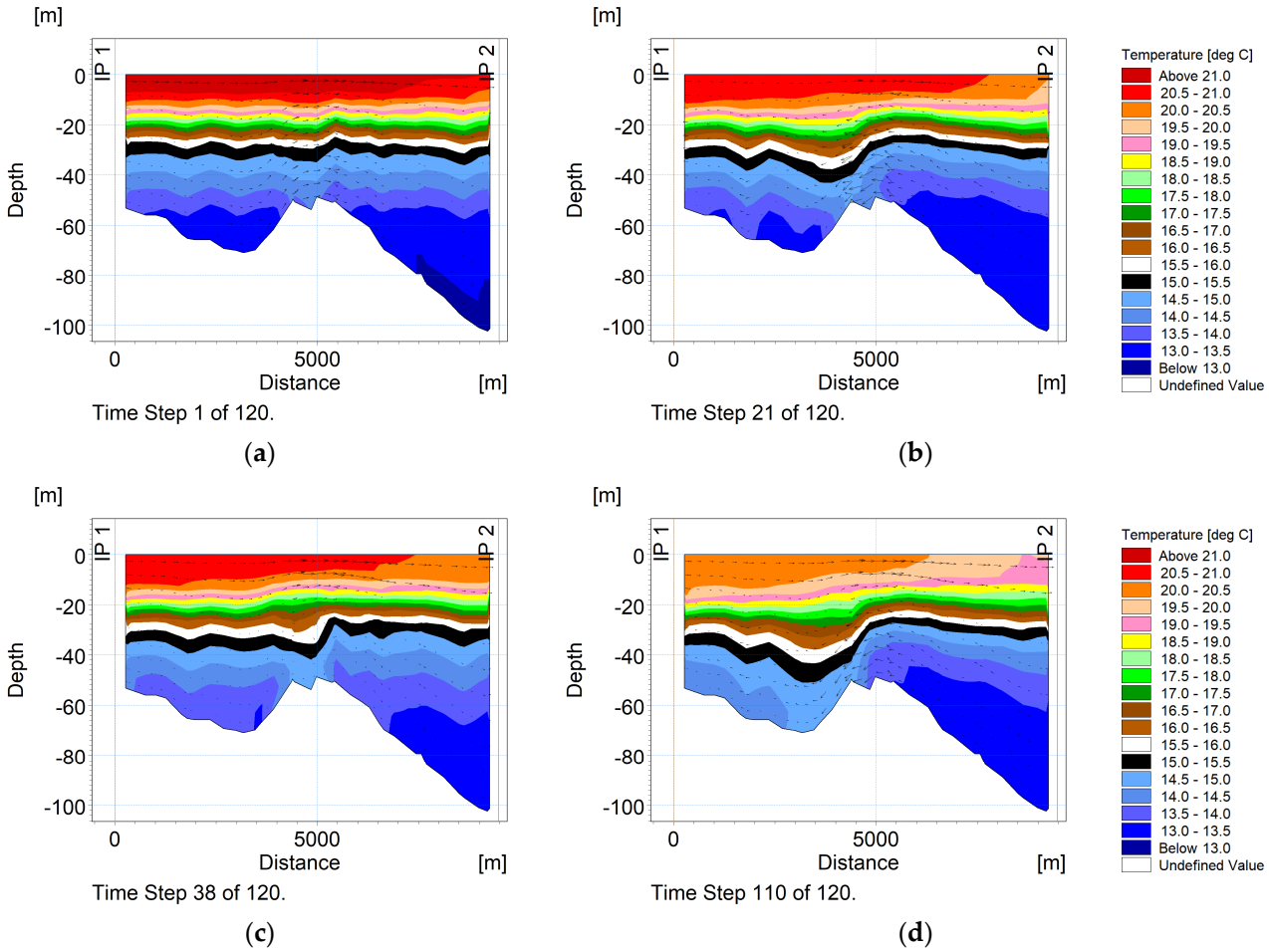


Figure 4. Vertical temperature distribution showing in different phases the motion of an internal wave at a cross-section along the Rio-Antirio strait. The reverse flow as well as the strong subsurface currents are evident. Isotherms drawn with 0.5 °C interval. The cross-section IP1-IP2 corresponds to Figure 2b.

In Figure 5a, the formation of the internal wave in the water column of the strait is given as a time evolution of thermal fluctuations for the total simulation period. It is noted that the depicted simulation results regard the center of the strait and present the change in temperature structure in characteristic sites over the flow depth, covering an area from the free surface to a few meters above the bottom of the strait. The time evolution of the temperature in these sites is provided in Figure 5b for the first twelve hours from the onset of the SW wind. Based on the simulations, it seems that the vertical temperature structure remains nearly constant for the first 6 h from the onset of the SW wind, whereas after 6 h, the internal wave motion gradually leads to a oscillation of the thermocline. Detailed observations of simulated thermal fluctuations in the water column reveal a wave-like amplitude of more than 20 m.

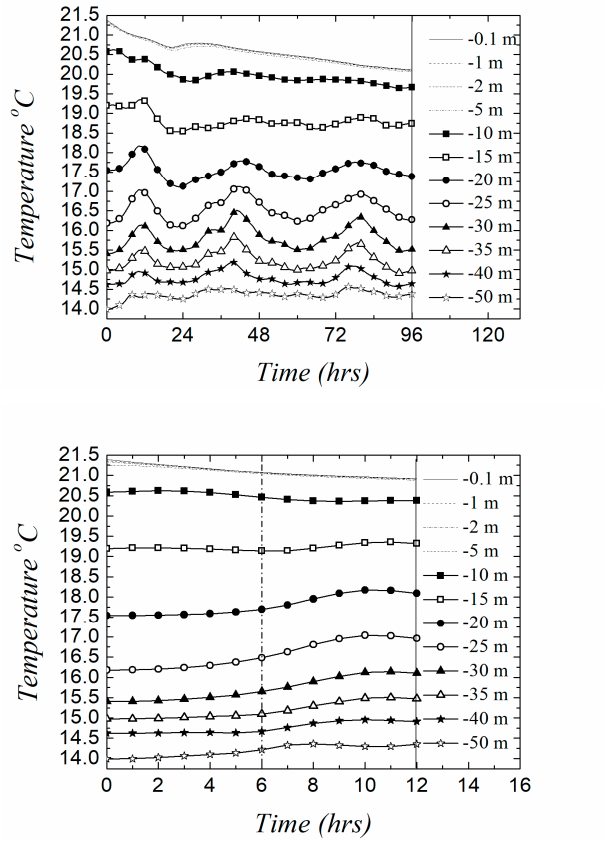


Figure 5. (**a**) Time evolution of thermal fluctuations in the center of the strait, where the temperature structure is given at characteristic locations above the flow depth. (**b**) Detail for the first 12 h from the wind onset.

The effect of subsurface/bottom currents, caused by the internal wave motion, is reflected in the calculation of the exchange flowrate. The evolution of the exchange flowrate at the examined strait for a SW wind of 4 m/s is presented in Figure 6. It is observed that for the wind-induced barotropic circulation, steady state is practically achieved within two days [49]. In contrast, for the baroclinic circulation, the evolution of the exchange flowrate shows some periodicity due to the action of the internal wave at the strait. In the latter case, the exchange flowrate closely resembles the one simulated for the tide-induced flow in the same basin.

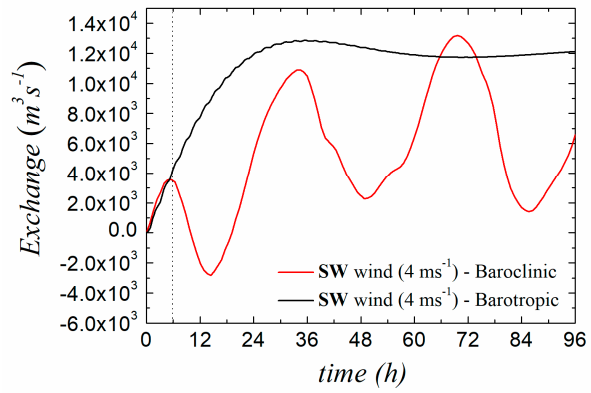


Figure 6. The hydraulic exchange flowrate at the Rio-Antirio strait due to a SW wind of 4 m/s for baroclinic and barotropic flow.

The previous behavior of the flow is also developed for the northeasterly (NE) wind of the same speed. In this case, however, the generation of the internal wave is calculated 48 h after the wind's onset. It is noted that the effect of stratification on the exchange flowrate is almost negligible for the first 24 h. The details of the initiation of the internal wave clearly depend on the conditions that exist upon the onset of the wind action and, hence, upon the initial conditions of the simulation. Therefore, it is concluded that the geometry that regards the strait induces differences on the generation and action of the internal wave, which depend on the direction from which the wind blows. Specifically, in the case of a constant NE wind, the exchange flowrate receives approximately equal values for the first day (0–24 h) as those obtained for the barotropic circulation. After the first day and up to the second one (24–48 h), the flow seems to be driven to a quasi-steady state, which closely resembles that of the barotropic circulation, achieving however a 15% lower average value of exchange flowrate compared to the corresponding value of the barotropic circulation. However, after the second day of wind action, the motion of internal waves begins, causing a subsurface change in the direction of the currents, which affect the exchange flowrate at the area of the strait, as seen in Figure 7.

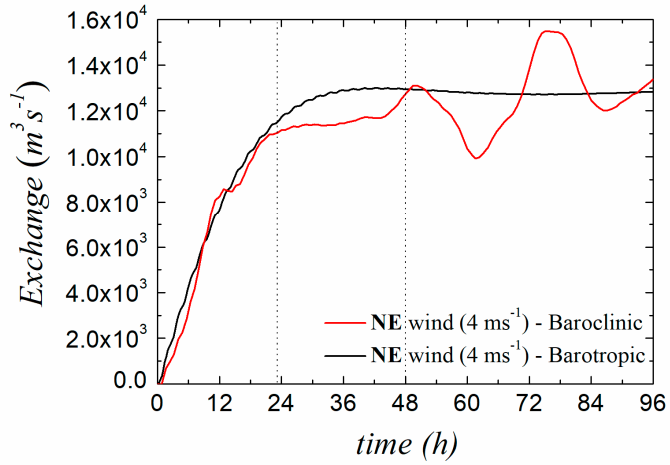
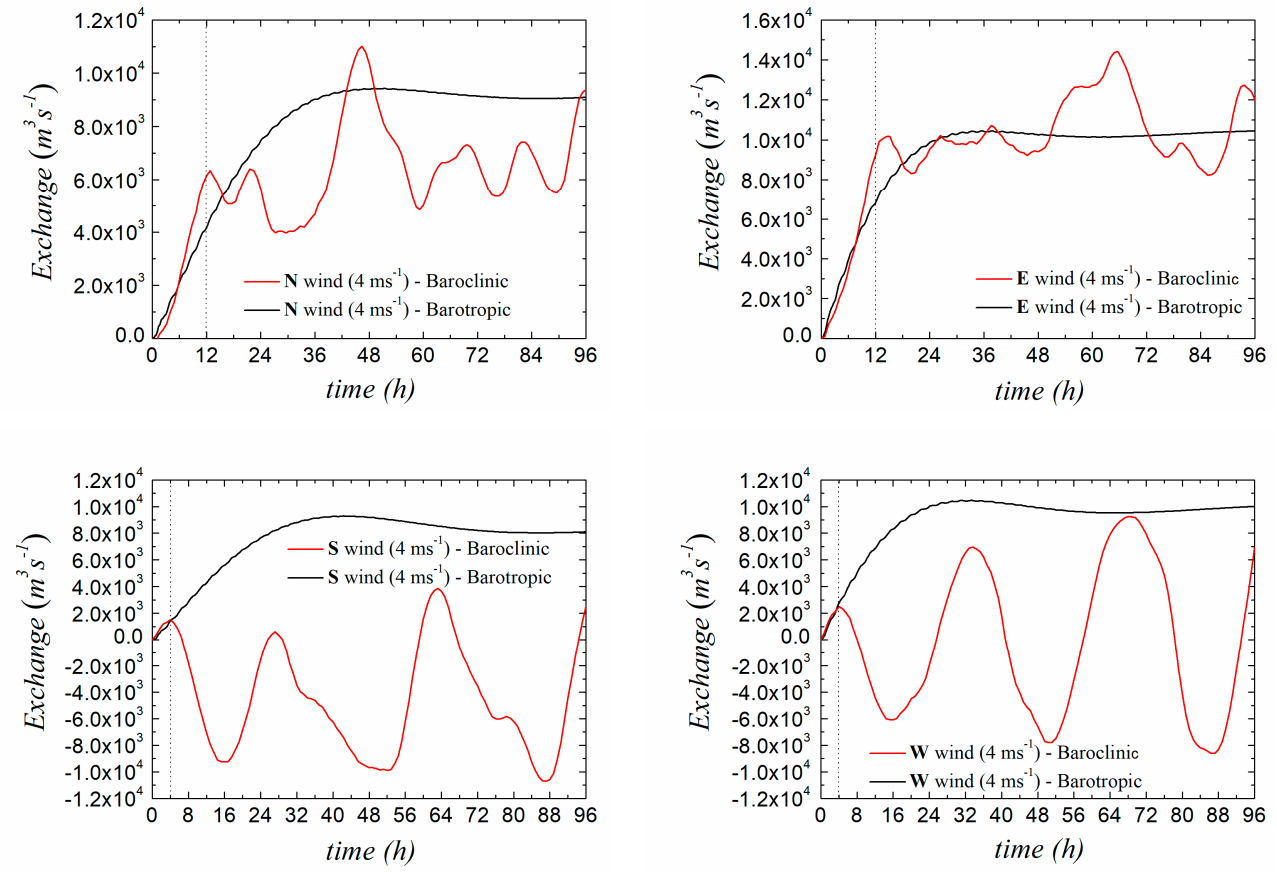
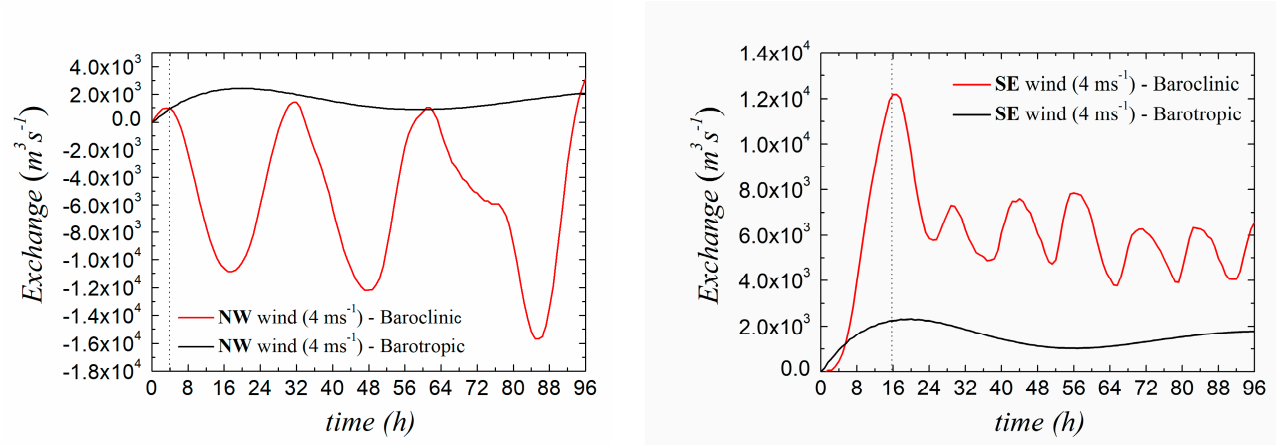


Figure 7. The hydraulic exchange flowrate at the Rio-Antirio strait due to a NE wind of 4 m/s for baroclinic and barotropic flow.

The effects of wind for northerly (N), easterly (E), southerly (S), and westerly (W) light winds of 4 m/s, i.e., regarding four characteristic directions of the wind in the wider area of the strait, are given in Figure 8a. The presence of the internal waves in the strait is reflected in the exchange flowrate that it is observed after approximately 12 h from the onset of northerly (N) and easterly (E) winds, and approximately 4 h from the onset of southerly (S) and westerly (W) winds. It is worth noting that when the wind blows from the north (N), northeast (NE), east (E), and southeast (SE), covering the eastern sector of the wind directions that includes the most frequent winds, i.e., ~52% of the total wind directions in the area, there is no net reverse flow in the strait. In these cases, however, the action of the internal waves was found to have a major effect on the magnitude of the horizontal U-velocity of the hypolimnetic waters, since the motion of the internal waves facilitates the wind-induced flow in the strait. On the contrary, for southerly (S), southwesterly (SW), westerly (W), and northwesterly (NW) winds, covering the western sector of the wind directions that includes winds with a frequency of ~30% of the total wind directions, the generation of internal waves leads to a purely reverse hypolimnetic flow in the strait area since the motion of the internal waves opposes the wind-induced flow in the strait (see Figure 3a for the case of SW wind).



(**a**)



(**b**)

Figure 8. (**a**). The hydraulic exchange flowrate at the Rio-Antirio strait due to main wind directions, i.e., N, E, S, W, of 4 m/s for baroclinic and barotropic flow. (**b**). The hydraulic exchange flowrate at the Rio-Antirio strait due to NW and SE winds of 4 m/s for baroclinic and barotropic flow.

Finally, the generation of internal waves was found to have a decisive effect on the exchange flowrate between the two gulfs for the NW and SE winds compared to the corresponding barotropic flow (Figure 8b). The latter marginally affects the exchange flowrate at the strait of Rio-Antirio, having a minor effect on the exchange flowrate between the gulfs.

Based on the numerical simulations for the wind-induced circulation, it is shown that the shear stress exerted by the wind on the free surface gradually generates a wave-like oscillation at the initial density stratification of the strait. Furthermore, wind direction as

well as strait geometry and topographic effects appear to remain critical parameters for the initiation and effects of internal waves for a steady light wind, as is considered here.

3.2.2. Tide-Induced Circulation

The simulation of the summer-stratified tidal flow presents the same structure as that of the internal waves and strong subsurface reverse flow in the strait. Under the condition of stratification, the tidal action was found to create internal waves higher than 20 m, regardless of the presence of wind. Based on the numerically predicted results, the internal waves' action affects the structure of the strait flow. The numerical predictions for the baroclinic flow propose that during the flood tide, and even in windless conditions, the generation of the internal waves in the strait causes a subsurface hypolimnetic inflow of colder waters from the deeper gulf into the shallower one, as well as strong bottom currents. Simultaneously, in the surface well-mixed waters, the current is directed to the Gulf of Corinth. In contrast, under the same conditions during the barotropic flow, the simulations propose that the currents at the straits are unidirectional throughout the strait's depth. Furthermore, despite the fact that the internal waves have a little effect on the net exchange flowrate between the gulfs, it causes a phase lag which is absent in the case of the barotropic flow. Based on the above, it is concluded that the action of the internal waves slightly affects the net exchange flowrate in the examined strait. It is also concluded that the wind effect on the exchange flowrate in the strait under the presence of tide was quite weak compared to the tidal effect, at least regarding the usual winds of the area (Figure 9).

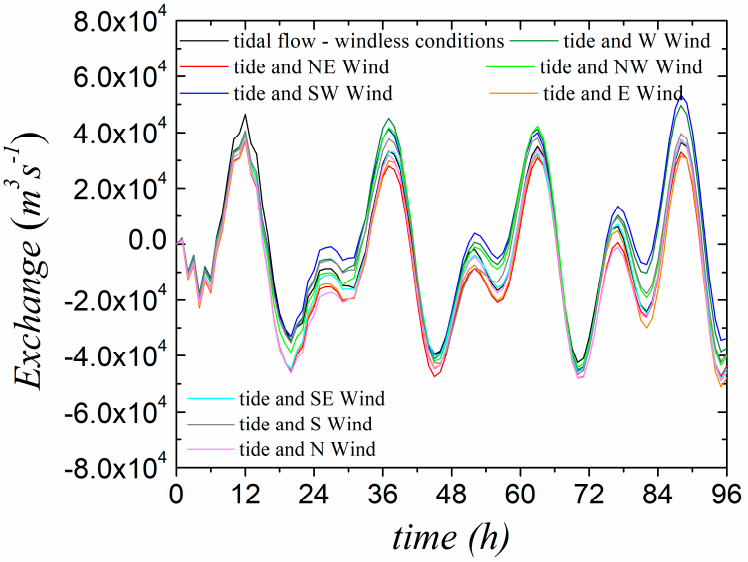


Figure 9. The hydraulic exchange flowrate at the Rio-Antirio strait due to a NW and SE winds of 4 m/s for baroclinic and barotropic flow.

Based on the numerical simulations for the tide-induced circulation, it is shown that the tidal forcing generates internal tides, i.e., internal waves in the strait area. The combined action of the wind was calculated to marginally affect the generation and action of internal waves. In this case, wind direction appears to have a limited effect on the internal waves' action for a steady light wind, as is considered here.

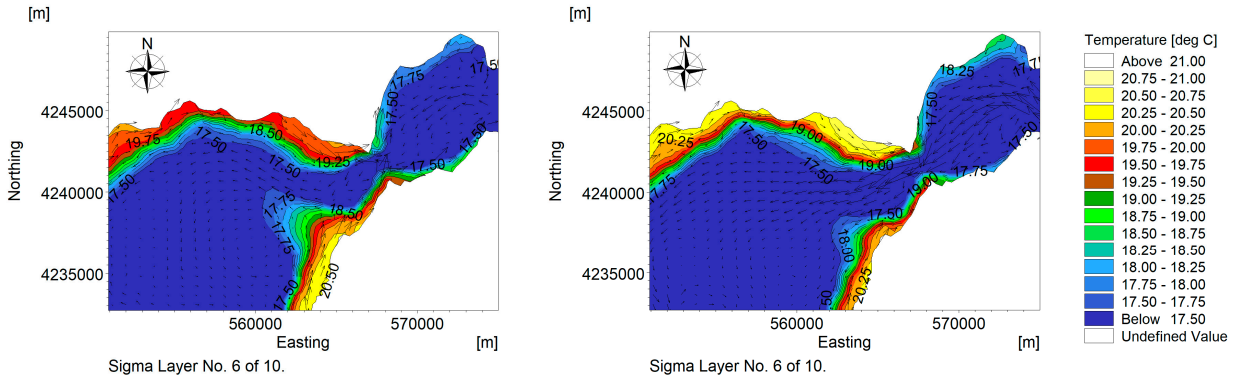
The characteristic numerically predicted results on the initiation of internal waves as well as the generation of reverse flow in subsurface (hypolimnetic) waters in the strait for wind- and tide-induced circulation, respectively, are summarized in Table 1.

Table 1. Simulated results of the examined scenarios for the wind- and tide-induced circulation.

	Wind-Induced Circulation		Tide-Induced Circulation
Direction (4 m/s Wind)	**Initiation of Internal Waves after Wind's Onset (h)**	**Reversed Subsurface (Hypolimnetic) Flow**	**Reversed Subsurface (Hypolimnetic) Flow**
N	12		√
NE	48		√
E	12		√
SE	16		√
S	4	√	√
SW	6	√	√
W	4	√	√
NW	4	√	√
Calm	-	-	√

3.3. Interplay of Coriolis Effect and Internal Waves

In the area away from the strait location, the circulation was found to be controlled by a complex interplay of the Coriolis effect and the internal waves' motion, which contribute to the development of complicated hydrodynamic processes in the wider area. As previously mentioned, wind forces on the surface of the basin result in the creation of internal waves in the strait, as clearly shown in Figure 4. It is also reminded that, based on the thermal fluctuations simulations, these internal waves have amplitudes higher than 20 m. The constant rising and falling of the thermocline plays a significant role in the water renewal upstream and downstream of the strait, acting nearly as a bellow that pumps water into and out of the Gulf of Patras. As water flows into and out of the Gulf of Patras, it is affected by the Coriolis force, resulting in an asymmetrical horizontal flow structure. This asymmetry is evident in Figure 10a and indicates the effect of the Coriolis force on the horizontal structure of the flow away from the strait area compared to the idealized case of Figure 10b, in which the Coriolis effect is neglected. As observed in Figure 10a, below the thermocline, subsurface colder waters that originated from the Gulf of Corinth are deflected to the right, mainly affecting the thermal structure of the northwestern coasts of the wider area of the strait, and to the west of Cape Antirio, leaving the southwestern coasts nearly unaffected to the west of Cape Rio.



(**a**) (**b**)

Figure 10. *Cont.*

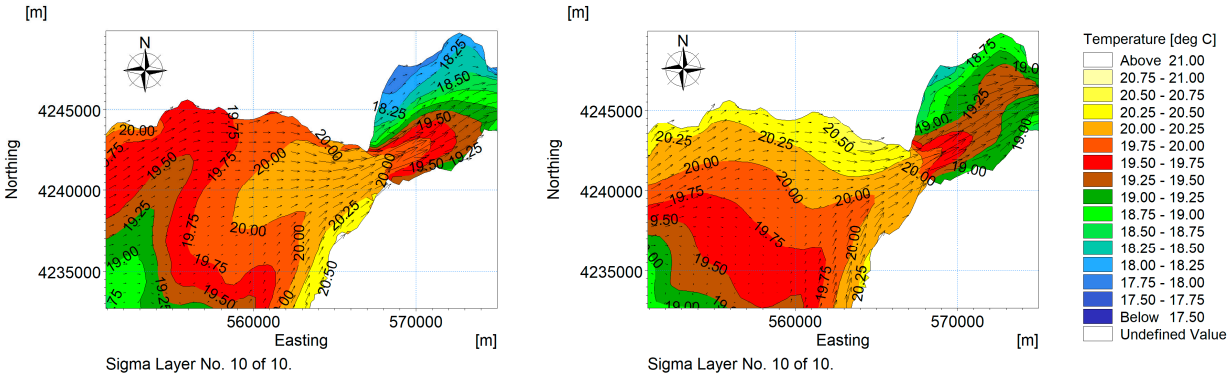


Figure 10. Calculated structure of the thermal stratification, induced by a 4 m/s southwesterly wind and the simultaneous action of internal waves below the thermocline (**a**) with and (**b**) without the Coriolis effect and at the free surface of the epilimnion (**c**) with and (**d**) without the Coriolis effect.

Above the thermocline, the wind-induced flow is formed as follows: As the thermocline moves (Figures 3a and 4), hypolimnetic colder water is drawn into the Gulf of Patras, while at the free surface, epilimnetic warmer water is forced into the Gulf of Corinth. These phenomena occur under the wind action in an easterly direction and mainly affect the southern coasts of the western tip of the Gulf of Corinth, i.e., the southern coasts of the Nafpaktos Bay. The Coriolis force deflects the surface thermal waters to the right considering the direction of propagation, resulting in generally warmer and faster coastal currents along the southern shores of the Bay, as shown in Figure 10c,d.

3.4. The Structure of Turbulence in the Strait

3.4.1. Wind-Induced Flow

For the wind-induced flow, the presence of the metalimnion zone limits the wind-generated turbulence in the upper well-mixed waters. As a result, turbulent viscosity attains higher values there. Furthermore, the action of internal waves as well as the subsequent vertical flow structure below the metalimnion, i.e., the generation of strong bottom currents, lead to a bottom-generated turbulence in the hypolimnetic colder waters. The turbulence intensity attains higher values there and so does the eddy viscosity; these values are of the same order of magnitude as those obtained in the case of the wind-generated turbulence at the free surface (Figure 11a). In contrast, in the barotropic flow, the wind-generated turbulence spreads uniformly within the layer where barotropic flow develops. It is worth noting that the area of the strait is quite limited, with a horizontal length scale of ~2 km. Thus, it is expected that the Coriolis effect will be limited to the region near the strait with increasing wind speed despite the overall Ro value. In this area, the wind-induced flow resembles that of an open channel rather than a geophysical flow, and the vertical eddy viscosity forms a parabolic-like structure, attaining higher values in the direction to which the wind is blowing and almost in the center of the flow depth (Figure 11b,c).

3.4.2. Tide-Induced Flow

The tidal turbulence is generated at the bottom and spreads towards the free surface layers of the water column, while the wind generated turbulence diffuses towards the lower layers. In the water body, the metalimnion acts as a separator zone, preventing the vertical mixing. Thus, the surface turbulence remains confined at the epilimnion and the tidal turbulence within the hypolimnion. The structure of the calculated eddy viscosity is as follows: Within the metalimnion, the eddy viscosity attains values approximately one order of magnitude lower than at the free surface and bottom, (Figure 12a). In contrast, the barotropic tidal flow allows vertical mixing from the bottom to the upper layers, leading to a nearly parabolic structure of vertical eddy viscosity profile, similar to that calculated for a

typical turbulent open-channel flow, (Figure 12b). Furthermore, the barotropic tidal flow leads to a change in the intensity of turbulence in the regions upstream and downstream of the strait due to the reversal of tidal currents in the strait. The vertical distribution of turbulent viscosity exhibits a parabolic behavior, the presence of which is due to the direction of the tidal flow. Consequently, this parabolic-like profile of eddy viscosity alternates upstream and downstream of the strait site, according to the direction of tidal currents (Figure 12b). Under the combined action of wind and tide, the turbulence diffuses freely from the free surface to the bottom, as well as from the bottom to the surface layers of the water column. Therefore, the distribution of turbulent viscosity shows a parabolic-like behavior, as in the case of pure tidal flow in the absence of wind, provided that the magnitude of the turbulent viscosity is affected by the wind forcing for the cases where the wind opposes or favors the direction of the tidal flow.

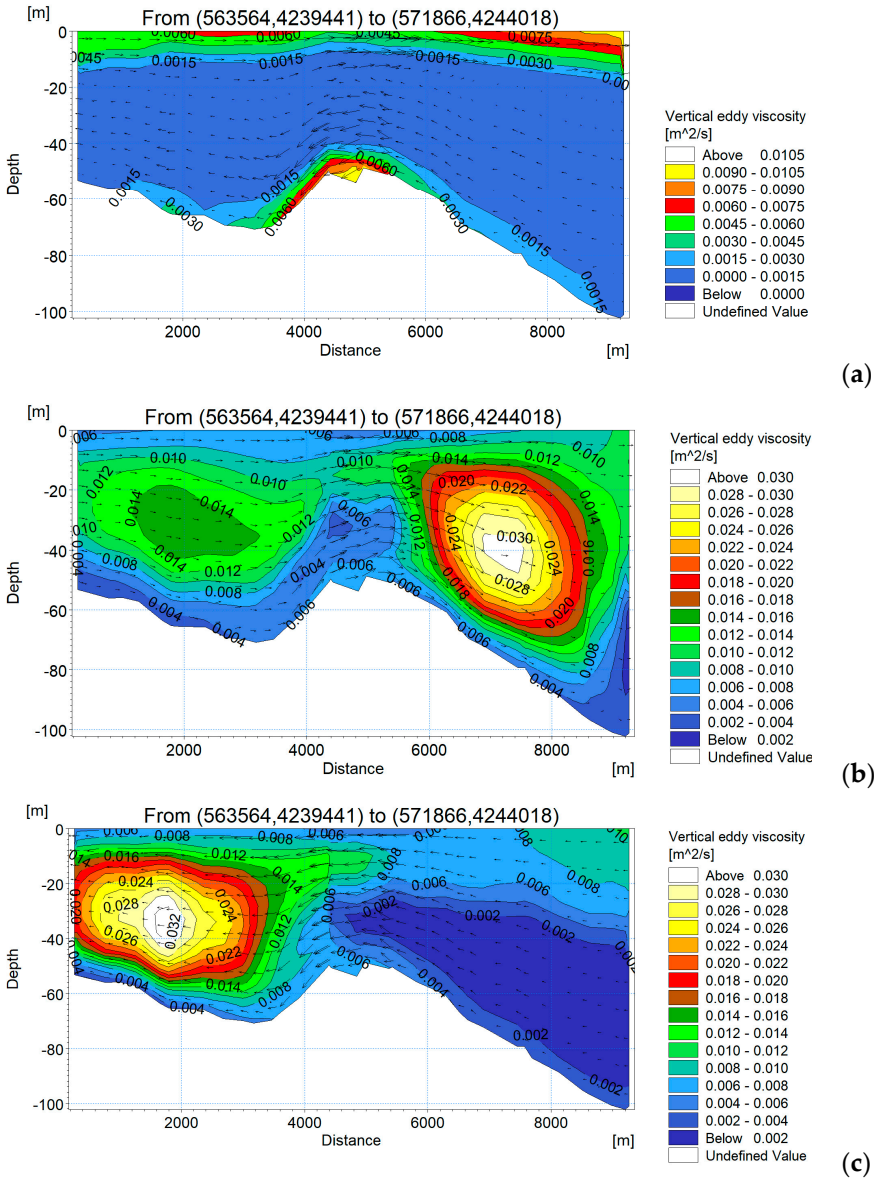


Figure 11. Vertical structure of turbulent eddy viscosity for the wind-induced (**a**) baroclinic circulation under SW wind, (**b**) barotropic circulation under SW wind, (**c**) barotropic circulation under NE wind.

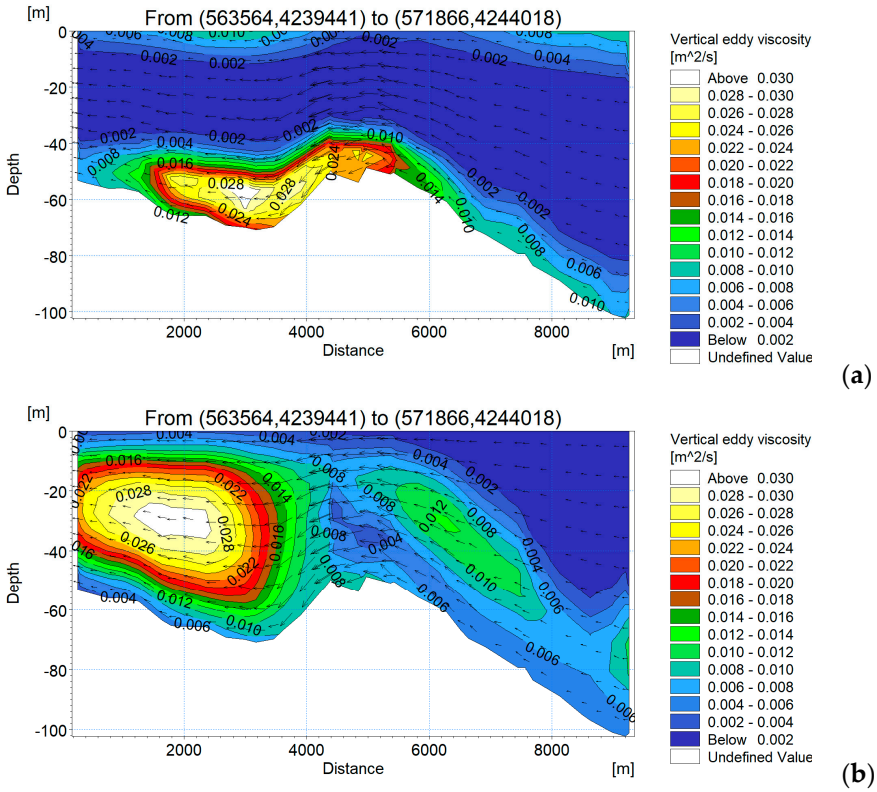


Figure 12. Vertical structure of turbulent eddy viscosity for windless condition. (**a**) Baroclinic tidal circulation. (**b**) Barotropic tidal circulation.

4. Conclusions

In this work, the structure of the flow, as well as the exchange flowrate and the turbulence intensity, in the Rio—Antirio strait under the effect of wind- and tide-induced internal waves was studied numerically. Based on the simulations, the following conclusions are drawn:

- Stratification plays an important role in the hydrodynamics of the strait, which leads to the generation of internal waves, locally affecting the structure of the flow;
- Wind-induced circulation has a critical effect in the wider area of the strait, causing strong wind-induced currents at the upper layer of the epilimnion. The action of internal waves causes strong subsurface currents' "pumping" of water from the deeper and colder gulf into the shallower one. On the free surface, the direction of the flow is driven by the wind action;
- For winds blowing from the eastern sector, there is no net reverse flow in the strait water column under the effect of internal waves. In these cases, the motion of the internal waves facilitates the wind-induced flow in the strait, as well as the magnitude of the hypolimnetic flow velocity. On the contrary, for winds covering the western sector, the generation of internal waves leads to a purely reverse flow in the strait area, since their motion opposes the dominant wind-induced flow in the strait;
- Tide-induced internal waves marginally affect the exchange flowrate in the Rio–Antirio strait. Under the tidal action, strong currents in the order of 1 m/s are generated at the upper layer of the epilimnion, while the effect of internal wave leads to the formation of subsurface currents with the opposite direction compared to the principal tidal direction of the flow in the strait. These currents also carry colder waters from the deeper gulf to the warmer one;
- Turbulence structure was estimated to be substantially affected by the action of internal waves in the strait. For the wind-induced flow, the action of internal waves leads to a bottom generated turbulence. For the tidal flow, the tide-generated turbulence

is restricted within the hypolimnion. In all the cases examined, the wind generated turbulence is restricted within the epilimnion;
- Under the influence of internal waves, the spatially varying current field in the strait reveals strong bottom currents, which in turn could be related to transport as well as dispersive phenomena in the vicinity of the strait.

Funding: This research received no external funding.

Institutional Review Board Statement: Not applicable.

Informed Consent Statement: Not applicable.

Data Availability Statement: All numerical data are available, please contact by e-mail nfou@uop.gr.

Acknowledgments: I would like to express my gratitude to the Danish Hydraulic Institute (DHI) for making available the 2023 version of MIKE 3 Flow Model FM (HD) (DHI Water and Environment, 2023).

Conflicts of Interest: The author declares no conflicts of interest.

References

1. Al Senafi, F.; Anis, A. Internal waves on the continental shelf of the Northwestern Arabian Gulf. *Front. Mar. Sci.* **2020**, *6*, 805. [CrossRef]
2. Holloway, P.E. Internal hydraulic jumps and solitons at a shelf break region on the Australian North West Shelf. *J. Geophys. Res. Ocean.* **1987**, *92*, 5405–5416.
3. Von Arx, W.S. *An Introduction to Physical Oceanography*; Addison-Wesley Publishing Company, Inc.: Boston, MA, USA, 1962; 422p.
4. Defant, A. *Physical Oceanography*; Pergamon Press: New York, NY, USA, 1961; Volume 2, 598p.
5. Leder, N. Wind-induced internal wave dynamics near the Adriatic shelf break. *Cont. Shelf Res.* **2002**, *22*, 445–463. [CrossRef]
6. Waterhouse, A.F.; MacKinnon, J.A.; Nash, J.D.; Alford, M.H.; Kunze, E.; Simmons, H.L.; Polzin, K.L.; Laurent, L.C.S.; Sun, O.M.; Pinkel, R.; et al. Global patterns of diapycnal mixing from measurements of the turbulent dissipation rate. *J. Phys. Oceanogr.* **2014**, *44*, 1854–1872. [CrossRef]
7. Legg, S.; Klymak, J. Internal hydraulic jumps and overturning generated by tidal flow over a tall steep ridge. *J. Phys. Oceanogr.* **2008**, *38*, 1949–1964. [CrossRef]
8. Apel, J.R. Oceanic Internal Waves and Solitons. An Atlas of Oceanic Internal Solitary Waves. 2020, Volume 1, pp. 1–40. Available online: https://www.internalwaveatlas.com/Atlas2_PDF/IWAtlas_Pg001_Background&Theory.pdf (accessed on 22 January 2024).
9. Laurent, L.S.; Alford, M.H.; Paluszkiewicz, T. An introduction to the special issue on internal waves. *Oceanography* **2012**, *25*, 15–19. [CrossRef]
10. Baines, P.G. *Topographic Effects in Stratified Flows*; Cambridge University Press: Cambridge, MA, USA, 1998; 500p.
11. Massel, S.R. *Internal Gravity Waves in the Shallow Seas*; Springer International Publishing: Berlin/Heidelberg, Germany, 2015.
12. Benilov, A.Y.; Solntseva, N.I.; Filyushkin, B.N. Relationship between the variability of the wind field and internal waves. *Oceanology* **1978**, *18*, 257–266.
13. LeBlond, P.H.; Mysak, L.A. *Waves in the Ocean*; Elsevier: Amsterdam, The Netherlands, 1981.
14. Morozov, E.G. *Oceanic Internal Tides: Observations, Analysis and Modeling. A Global View*; Springer: Cham, Switzerland, 2018; 304p. [CrossRef]
15. Koohestani, K.; Stepanyants, Y.; Allahdadi, M.N. Analysis of Internal Solitary Waves in the Gulf of Oman and Sources Responsible for Their Generation. *Water* **2023**, *15*, 746. [CrossRef]
16. Wang, C.; Wang, X.; Da Silva, J.C. Studies of internal waves in the strait of Georgia based on remote sensing images. *Remote Sens.* **2019**, *11*, 96. [CrossRef]
17. Khimchenko, E.E.; Frey, D.I.; Morozov, E.G. Tidal internal waves in the Bransfield Strait, Antarctica. *Russ. J. Earth Sci.* **2020**, *20*, 6. [CrossRef]
18. Purwandana, A.; Edikusmanto, E.; Utari, P.A.; Lestiana, H.; Saputra, O.F.; Sari, Q.W. Observation of Internal Solitary Waves near Its Generation Site in the Lombok Strait, Indonesia. *Positron* **2023**, *13*, 95–103. [CrossRef]
19. Brandt, P.; Rubino, A.; Quadfasel, D.; Alpers, W.; Sellschopp, J.; Fiekas, H.V. Evidence for the influence of Atlantic-Ionian Stream fluctuations on the tidally induced internal dynamics in the Strait of Messina. *J. Phys. Oceanogr.* **1999**, *29*, 1071–1080. [CrossRef]
20. Vlasenko, V.; Brandt, P.; Rubino, A. Structure of large-amplitude internal solitary waves. *J. Phys. Oceanogr.* **2000**, *30*, 2172–2185. [CrossRef]
21. Sangra, P.; Basterretxea, G.; Pelegri, J.L.; Aristegui, J. Chlorophyll increase due to interna1 waves on the shelf break of Gran Canaria (Canary Islands). *Sci. Mar.* **2001**, *65* (Suppl. S1), 89–97. [CrossRef]
22. Rinke, K.; Bner, I.H.; Petzoldt, T.; Rolinski, S.; Nig-Rinke, M.K.; Post, J.; Lorke, A.; Benndorf, J.R. How internal waves influence the vertical distribution of zooplankton. *Freshw. Biol.* **2007**, *52*, 137–144. [CrossRef]

23. Garwood, J.C.; Musgrave, R.C.; Lucas, A.J. Life in Internal Waves. *Oceanography* **2020**, *33*, 38–49. [CrossRef]
24. Ziegenbein, J. Short internal waves in the Strait of Gibraltar. *Deep Sea Res. Oceanogr. Abstr.* **1969**, *16*, 479–487. [CrossRef]
25. Boyce, F.M. Internal waves in the Straits of Gibraltar. *Deep Sea Res. Oceanogr. Abstr.* **1975**, *22*, 597–610. [CrossRef]
26. Watson, G.; Robinson, I.S. A study of internal wave propagation in the Strait of Gibraltar using shore-based marine radar images. *J. Phys. Oceanogr.* **1990**, *20*, 374–395. [CrossRef]
27. Pistek, P.; La Violette, P.E. Observations of the suppression of tide-generated nonlinear internal wave packets in the Strait of Gibraltar. *J. Mar. Syst.* **1999**, *20*, 113–128. [CrossRef]
28. Morozov, E.G.; Trulsen, K.; Velarde, M.G.; Vlasenko, V.I. Internal tides in the Strait of Gibraltar. *J. Phys. Oceanogr.* **2002**, *32*, 3193–3206. [CrossRef]
29. Vázquez, A.; Bruno, M.; Izquierdo, A.; Macías, D.; Ruiz-Cañavate, A. Meteorologically forced subinertial flows and internal wave generation at the main sill of the Strait of Gibraltar. *Deep Sea Res. Part I Oceanogr. Res. Pap.* **2008**, *55*, 1277–1283. [CrossRef]
30. Griffa, A.; Marullo, S.; Santoleri, R.; Viola, A. Internal nonlinear tidal waves generated at the Strait of Messina. *Cont. Shelf Res.* **1986**, *6*, 677–687. [CrossRef]
31. Sapia, A.; Salusti, E. Observation of nonlinear internal solitary wave trains at the northern and southern mouths of the Strait of Messina. *Deep Sea Res. Part A. Oceanogr. Res. Pap.* **1987**, *34*, 1081–1092. [CrossRef]
32. Alpers, W.; Brandt, P.; Rubino, A.; Backhaus, J.O. Recent contributions of remote sensing to the study of internal waves in the straits of Gibraltar and Messina. *Bull. -Inst. Oceanogr. Monaco-Numero Spec.* **1996**, *17*, 21–40.
33. Brandt, P.; Rubino, A.; Alpers, W.; Backhaus, J.O. Internal waves in the Strait of Messina studied by a numerical model and synthetic aperture radar images from the ERS 1/2 satellites. *J. Phys. Oceanogr.* **1997**, *27*, 648–663. [CrossRef]
34. Casagrande, G.; Varnas, A.W.; Stéphan, Y.; Folégot, T. Genesis of the coupling of internal wave modes in the Strait of Messina. *J. Mar. Syst.* **2009**, *78*, S191–S204. [CrossRef]
35. Droghei, R.; Falcini, F.; Casalbore, D.; Martorelli, E.; Mosetti, R.; Sannino, G.; Santoleri, R.; Chiocci, F.L. The role of Internal Solitary Waves on deep-water sedimentary processes: The case of up-slope migrating sediment waves off the Messina Strait. *Sci. Rep.* **2016**, *6*, 36376. [CrossRef] [PubMed]
36. Oddo, P.; Poulain, P.M.; Falchetti, S.; Storto, A.; Zappa, G. Internal tides in the central Mediterranean Sea: Observational evidence and numerical studies. *Ocean Dyn.* **2023**, *73*, 145–163. [CrossRef]
37. Drakopoulos, P.G.; Lascaratos, A. A preliminary study on the internal tides of the gulfs of Patras and Korinthos, Greece. *Cont. Shelf Res.* **1998**, *18*, 1517–1529. [CrossRef]
38. Rubi, R.; Hubert-Ferrari, A.; Fakiris, E.; Christodoulou, D.; Dimas, X.; Geraga, M.; Papatheodorou, G.; Caterina, B. Hydrodynamics and sedimentary processes in the modern Rion strait (Greece): Interplay between tidal currents and internal tides. *Mar. Geol.* **2022**, *446*, 106771. [CrossRef]
39. Google Earth Pro, Version 7.3.6.9345. Available online: https://www.google.com/earth/versions/#earth-pro (accessed on 22 January 2024).
40. Papailiou, D.D. *Oceanographical Study in Patras Gulf Waters for Pollution Management*; Department of Mechanical Engineering, University of Patras: Patras, Greece, 1982; Volume II. (In Greek)
41. Friligos, N.; Theoharis, A.; Georgopoulos, D. Preliminary chemical and physical observations during summer 1980 on a silled embayment in the Ionian Sea. *Vie Et Milieu* **1985**, *35*, 115–125.
42. Lascaratos, A.; Salusti, E.; Papageorgaki, G. Wind-induced upwellings and currents in the gulfs of Patras, Nafpaktos and Korinthos, Western Greece. *Oceanol. Acta* **1989**, *12*, 159–164.
43. Poulos, S.E.; Collins, M.B.; Pattiaratchi, C.; Cramp, A.; Gull, W.; Tsimplis, M.; Papatheodorou, G. Oceanography and sedimentation in the semi-enclosed, deep-water Gulf of Corinth (Greece). *Mar. Geol.* **1996**, *134*, 213–235. [CrossRef]
44. Hadjitheodorou, C.; Antonopoulos, I. *Investigation and Analysis of Stability and Mechanical Behaviour of the Coastal Zone in the Area of Rion Antirion*; Final Report; Department of Civil Engineering, University of Patras: Patras, Greece, 1989.
45. Antonopoulos, J.; Ilias, D.; Papageorgiou, K.; Ahmed, S. *Investigation of the Anemological Field in the Area of Rio-Antirio for the Bridging Project*; Final Report, Ministry of Environment, Physical Planning and Public Works Directorate D1; University of Patras, Department of Civil Engineering: Patras, Greece, 1992. (In Greek)
46. Antonopoulos, J.; Grigoropoulos, S.; Tsonis, S.; Yannopoulos, P. *Research Investigation of Physical-Chemical Parameters of Seawater and Its Biological Pollution Potential on Underwater Construction in the Area of Rio-Antirio for the Bridge Project*; Final Report: 1. Physical-Chemical Parameters of Seawater, Ministry of Environment, Physical Planning and Public Works-Directorate D1; University of Patras, Department of Civil Engineering: Patras, Greece, 1992. (In Greek)
47. Hadjitheodorou, C.; Antonopoulos, J.; Lascaratos, A.; Papageorgiou, E.; Papageorgiou, K.; Trova, E. *Investigation of the Sea Currents in the Area of Rio-Antirio for the Bridging Project*; Final Report, Ministry of Environment, Physical Planing and Public Works-Directorate D1; University of Patras, Department of Civil Engineering: Patras, Greece, 1992. (In Greek)
48. Fourniotis, N.T. Three-Dimensional Numerical Simulation of the Hydrodynamic Circulation in the Gulf of Patras, with Emphasis on the Currents in the Coastal Zone of the Port of Patras. Ph.D. Thesis, Department of Civil Engineering, University of Patras, Patras, Greece, 2009. (In Greek).
49. Fourniotis, N.T.; Horsch, G.M. Three-dimensional numerical simulation of wind-induced barotropic circulation in the Gulf of Patras. *Ocean Eng.* **2010**, *37*, 355–364. [CrossRef]
50. Fourniotis, N.T.; Horsch, G.M. Baroclinic circulation in the Gulf of Patras (Greece). *Ocean Eng.* **2015**, *104*, 238–248. [CrossRef]

51. Horsch, G.M.; Fourniotis, N.T. Wintertime Tidal Hydrodynamics in the Gulf of Patras, Greece. *J. Coast. Res.* **2017**, *33*, 1305–1314. [CrossRef]
52. Achilleopoulos, P. Tides in Gulfs and Straits of Western Greece. Ph.D. Thesis, University of Patras, Department of Geology, Patras, Greece, 1990; 265p. (In Greek).
53. DHI Water and Environment. *MIKE 3 Flow Model FM, Hydrodynamic Module*; User Guide; DHI: Singapore, 2023; p. 158.
54. Smagorinsky, J. General circulation experiments with the primitive equations I. The basic experiment. *Mon. Weather Rev.* **1963**, *91*, 99–165. [CrossRef]
55. Rodi, W. *Turbulence Models and Their Applications in Hydraulics*; IAHR: Delft, The Netherlands, 1984.
56. Roe, P.L. Approximate Riemann solvers, parameter vectors and difference-schemes. *J. Comput. Phys.* **1981**, *43*, 357–372. [CrossRef]
57. Fourniotis, N.T. Erosion of the Thermocline in the Gulf of Patras, due to a Severe Wind event. *Glob. Nest J.* **2018**, *20*, 136–146.
58. Wadzuk, B.M.; Hodges, B.R. Comparing hydrostatic and non-hydrostatic Navier Stokes models of internal waves. In *Proceedings of the 16th ASCE Engineering Mechanics Conference, Seattle, WA, USA, 16–18 July 2003*; Electronic Proceedings; University of Washington: Seattle, WA, USA; 4p.
59. Hodges, B.R.; Laval, B.; Wadzuk, B.M. Numerical error assessment and a temporal horizon for internal waves in a hydrostatic model. *Ocean Model.* **2006**, *13*, 44–64. [CrossRef]
60. Wadzuk, B.M.; and Hodges, B.R. Hydrostatic versus Nonhydrostatic Euler-Equation Modeling of Nonlinear Internal Waves. *J. Eng. Mech.* **2009**, *135*, 1069–1080. [CrossRef]
61. Álvarez, Ó.; Izquierdo, A.; González, C.J.; Bruno, M.; Mañanes, R. Some considerations about non-hydrostatic vs. hydrostatic simulation of short-period internal waves. A case study: The Strait of Gibraltar. *Cont. Shelf Res.* **2019**, *181*, 174–186. [CrossRef]
62. Zamani, B.; Koch, M. Comparison between two hydrodynamic models in simulating physical processes of a reservoir with complex morphology: Maroon Reservoir. *Water* **2020**, *12*, 814. [CrossRef]

Disclaimer/Publisher's Note: The statements, opinions and data contained in all publications are solely those of the individual author(s) and contributor(s) and not of MDPI and/or the editor(s). MDPI and/or the editor(s) disclaim responsibility for any injury to people or property resulting from any ideas, methods, instructions or products referred to in the content.